ELSEVIER

Chemical Engineering Journal 90 (2002) 149–164

Chemical Engineering Journal

www.elsevier.com/locate/cej

Kinetics of the hydroxylation of benzene with N_2O on modified ZSM-5 zeolites

A. Reitzmann*, E. Klemm, G. Emig

Institute of Technical Chemistry I, University of Erlangen-Nuremberg, Egerland Street 3, D-91058 Erlangen, Germany

Abstract

A detailed kinetic study of the hydroxylation of benzene to phenol using nitrous oxide (N_2O) is performed on different, well characterised modifications of ZSM-5 type zeolites. After process studies in a fixed bed reactor for the first time a recycle reactor (Berty-type) is successfully used in direct measurements of the molar rates of reactant consumption and product formation. From those data, an extended reaction network is developed which contained mechanistic steps derived from additional studies. Besides the formation of a chemisorbed, monoatomic oxygen species from N_2O and phenol formation, it can be shown that a consecutive reaction of phenol without the participation of oxygen and a non-selective oxygenation of strongly adsorbed hydrocarbons by oxygen play an important role. The former step is attributed to the accumulation of phenol inside the ZSM-5 crystal due to strong adsorption and slow diffusion of phenol. The latter step results in an accumulation of oxygen within the adsorbed hydrocarbon species until a critical oxygen content is reached and total oxidation starts. An isothermal two-site kinetic model is deduced containing the sorption of the reactants and products. The values of the model parameters allow a comparison of the efficiency of the catalysts on the rates of each step. Simulations of the selectivity–conversion behaviour impressively demonstrate the quality of the kinetic model as predictive tool for process studies.
© 2002 Elsevier Science B.V. All rights reserved.

Keywords: Benzene hydroxylation; Phenol synthesis; Nitrous oxide; ZSM-5 zeolites; Recycle reactor (Berty-type); Kinetic modelling; Kinetic parameter estimation; Reactor simulation

1. Introduction

The direct synthesis of phenol from benzene is one of the top challenges in industrial bulk chemistry [1]. As an alternative to the traditional Cumene process, the coupled production of acetone can be avoided which is detrimental from the economic point of view [2,3]. The most promising results in direct hydroxylation of benzene have been obtained only with N_2O as oxidant, so far, and with ZSM-5 zeolites as catalysts. More than 50 scientific publications (e.g. reviews of Panov et al. [4] and Panov [5]) can be found in open literature, which mainly focuses on the influence of different ZSM-5 modifications on attainable conversions and selectivities. The mechanism of the whole process is mainly reduced on the decomposition of nitrous oxide forming a monoatomic oxygen species. However, the discussion about the responsible active sites for this step is still a controversy: Ironoxoclusters [4,6] Lewis acidic aluminium sites in framework [7,8] and extraframework position of the zeolite [9] are conceivable possibilities.

The generally accepted steps in the reaction network are shown in Fig. 1.

- Activation of N_2O forming a monoatomic, chemisorbed oxygen species (Z_1–O) upon release of nitrogen [10–13].
- Reaction of benzene with the oxygen species to phenol. [4,14].

The second step not only contains the phenol formation itself, but also the desorption of this product from the active site and the diffusion out of the zeolite channels. These steps are important for the kinetics of the process because of the relatively strong interaction of phenol with the zeolite. Investigations of the aromatic alkylation using different alkylation agents and benzene/phenol mixtures lead to similar conclusions [15,16]. While the sorption and diffusion of benzene using different ZSM-5 zeolites is extensively investigated (e.g. [17,18]), for phenol no quantitative results like sorption constants, enthalpies and diffusion coefficients are reported in literature. Sorption simulations with the Cerius^2 software by our group enabled a description of the interaction of several benzene–phenol mixtures with different ZSM-5 modifications [19]. Transient studies in the

* Corresponding author. Present address: Institute for Chemical Process Engineering, University of Karlsruhe, Kaiser Street 12, D-76131 Karlsruhe, Germany. Tel.: +49-721-608-3848; fax: +49-721-608-6118.
E-mail address: andreas.reitzmann@ciw.uni-karlsruhe.de (A. Reitzmann).

1385-8947/02/$ – see front matter © 2002 Elsevier Science B.V. All rights reserved.
PII: S1385-8947(02)00076-1

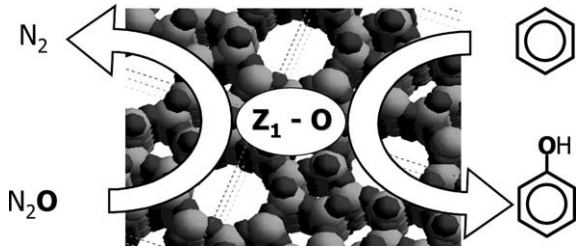

Fig. 1. General reaction scheme of the benzene hydroxylation to phenol using nitrous oxide (N_2O) on ZSM-5 type zeolites.

TAP reactor [12,13] and experiments with separated oxidation and reduction cycles [20] have supported the kinetic importance of the phenol sorption in the zeolite.

Besides the growing scientific understanding of the benzene hydroxylation with N_2O, many patents from different companies elucidate the high industrial potential of this process (e.g. [21–25]). This can be realised from a pilot plant operation of Solutia built in 1998 with an ambitious goal to integrate a direct phenol synthesis in the process for manufacturing adipic acid [3]. Therefore, the waste gas containing up to 50% N_2O should be used as an inexpensive source for an alternative oxidant demonstrating an example of process integrated environmental protection [26].

Due to industrial relevance, it seems astonishing that almost no detailed kinetic studies of the direct benzene hydroxylation have been published so far. We have already reported several preliminary kinetic models, which describe the experimental results using zeolites of type H-(Ga)ZSM-5 in a fixed bed reactor in 1997 and 1998 [27,28]. Recently, Louis et al. have also published kinetic studies using a fixed bed reactor filled with a structured catalyst packing where H-ZSM-5 is coated on stainless steel grids [29].

In the present paper, it will be shown how an extended reaction network can be deduced from kinetic studies performed in a recycle reactor of Berty-type and a fixed bed reactor with plug-flow behaviour using well-characterised zeolite samples. The development of this reaction network including several mechanistic steps combines all informations derived from earlier detailed studies fixed bed reactor [20], in the TAP reactor [12,13] and by sorption simulations [19]. On this basis, a kinetic model is developed which enables to quantify the rates of all relevant steps of the reaction network. These investigations and a detailed catalyst characterisation offers the possibility to follow a mechanistic approach without statistical model discrimination. All model parameters were estimated by non-linear regression of the measured reactant and product concentrations in both the reactors. The application of the model for different ZSM-5 type zeolite modifications illustrates the influence of the zeolite composition on the values of the kinetic parameters. By simulations using the kinetic model, it can be shown how the feed composition influences on the conversion–selectivity behaviour concerning benzene and N_2O for each catalyst.

2. Experimental

2.1. Catalysts preparation and characterisation

2.1.1. Preparation

As starting material, zeolites of ZSM-5 type in the Na-form (SN55) and in the NH_4-form (SM55) are used, which has been supplied by Dr. Tissler of AlsiPenta GmbH. These have been synthesised without using a template [30]. The NH_4-form is calcined in air at 550 °C for 3 h to get the protonated form. Iron is introduced by liquid ion-exchange method, which has already been described [31] and has been used by other groups in a similar way [32–34]. The suspension (100 ml of a 0.2 M solution of $Fe(NO_3)_3$, 10 g zeolite) is continuously stirred at 60 °C for 6 h. This procedure is repeated twice with a fresh $Fe(NO_3)_3$ solution. Finally, the zeolite is thoroughly washed with distilled water, as long as no more nitrate is detectable in the filtrate. Subsequently, both zeolites, the protonated and the iron-containing are activated ex situ by calcination in air for 12 h at 900 °C (rate 10 K/min). In a previous investigation, we found out that this procedure leads to optimum conversions and selectivities of this zeolite [20,31]. In the following, the protonated sample is designated as H-(Al)ZSM-5, and the iron exchanged sample as Fe-(Al)ZSM-5. Prior to the catalytic runs, the samples were pelletised without the binder and crushed to a size fraction of 0.7–1.0 mm.

2.1.2. Characterisation

The elementary composition of the zeolites is determined by X-ray fluorescence (XRF) of the powder and atomic emission spectroscopy with inductively coupled plasma (AES–ICP) of the dissolved samples.

Sorption measurements are carried out by the means of physisorption of nitrogen at 77 K to obtain the micropore volume of the zeolites (ASAP-2000 Micromeritics). For the qualification, the *t*-plot method was used [35].

Powder X-ray diffraction (XRD) data are collected in the 2θ range of 3–53° (steps: 0.02°) using monochromatic Cu Kα radiation (Phillips X'Pert pro). Crystallinities are determined by the method of Bergk and Schwieger in terms of Q_{Al}-values using α-Al_2O_3 as an external standard [36].

Coordination of present aluminium species were determined by ^{27}Al-MAS-NMR (Bruker NMR MSL-400; resonance frequency, 104.3 MHz). The change in framework Si/Al ratio after any sample treatment is calculated by determining the peak area at a chemical shift of 55 ppm (mathematical deconvolution using Gaussian functions), and relating it to that of the parent sample. The amount of Brønsted acidic sites is investigated by temperature programmed desorption of ammonia (NH_3-TPD) [37] using the catalyst characterisation system AMI-100 (ALTAMIRA Instruments). The amount of desorbed ammonia in the high temperature region is quantified by applying a pulse calibration method. The exact procedure is given elsewhere [38].

2.2. Apparatus and procedure for kinetic studies

The apparatus for the catalytic and kinetic measurements contains two different reactors which can be used optionally. In both reactors, the molar fractions, $x(i)$, of benzene and nitrous oxide were varied in the range of 0.02–0.11 and 0.02–0.25, respectively, at atmospheric pressure and a temperature of 400 °C. Nitrogen was used as inert balance. Reduced factorial experiments are performed in both reactors which are related to feed composition of 4 mol% N_2O ($x(N_2O) = 0.04$) and 4 mol% benzene ($x(B) = 0.04$) as fixed point.

2.2.1. Fixed bed reactor with plug-flow behaviour (PFR; length, 250 mm; i.d., 17.4 mm)

The modified residence time (τ_{mod} = mass of catalyst/total molar feed stream) is varied in the range of 78–156 g min/mol by variation of the total molar feed at a constant catalyst mass of 2 g. This corresponds to a fluid-1 dynamic residence time in the range of 2.5–5 s (τ = total volume stream/reactor volume) at 400 °C. The weight hourly space velocity (WHSV) related to liquid benzene varies from 1 to 5.5 h^{-1} depending on the feed concentration of benzene.

The reactor shows plug-flow behaviour at the chosen process conditions with Bodenstein numbers higher than 100 [39]. Moreover, it can be calculated via the criterion of Mears [40] that the axial dispersion can be neglected in the reactor balance at benzene and N_2O conversions lower than 95%. Thus, the plug-flow model can be used to describe the fixed bed reactor:

$$\frac{dx(i)}{d\tau_{mod}} = \sum_j \nu_{ij} R_j = R_i \quad (1)$$

Since the catalyst particles are smaller than 1 mm, no bypassing near the wall must be taken into account ($d_R/d_p > 10$) [41,42]. Temperature can be measured via an internal thermocouple to monitor the heat production during the reaction.

2.2.2. Recycle reactor of Berty-type (internal recycle)

The modified residence time (τ_{mod}) is 137 g min/mol at a catalyst mass of 1.88 g. The fluid dynamic residence time is about 42 s. The WHSV related to liquid benzene varies from 0.5 to 4 h^{-1} depending on the feed concentration of benzene. The recycle reactor shows the behaviour of an ideally continuous stirred tank reactor (CSTR), which has been proven by measuring the residence time distribution. Additionally, it is important to avoid concentration and temperature gradients in the CSTR, which can be controlled by the recycle ratio in certain limits. Theoretically, a minimum recycle ratio of 60 has been calculated via the criteria of Luft and Herbertz for the highest measured conversion as most critical cases [43], which can be reached with a turbine frequency of 150 Hz. It has been experimentally checked that the external diffusional limitations can be excluded at this recycle ratio because of sufficiently high gas velocities. The temperature gradient is measured on-line by two thermocouples above and below the catalyst basket.

The reactor balance of the CSTR can be represented by

$$\frac{x(i,0) - x(i)}{\tau_{mod}} = \sum_j \nu_{ij} R_j = R_i \quad (2)$$

where $x(i,0)$ is the molar fraction of the chemical species i in the feed and $x(i)$ in the reactor.

The concentrations of reactants and all products were analysed by two gas chromatographs, a Hewlett Packard HP 58990 Series II Plus (columns: PoraPlot Q, molecular sieve 5 Å, series bypass mode; detectors: FID, TCD) and a Chrompack micro-gas chromatograph CP-2002 (column: PoraPlot Q; detector: TCD) both measuring in on-line mode. During the regeneration period, CO_2 can be analysed very quickly with the micro-gas chromatograph (analysis time 90 s) to consider the carbon deposits on the catalyst surface into the carbon balance [20]. The whole set-up works fully automated, controlling temperature, feed composition and gas analysis by a personal computer.

The non-linear regression of the measured molar fractions of the reactants (benzene, N_2O) and of the main products (phenol and benzoquinone as main byproduct) is performed with the SIMUSOLV software (DOW Chemical Company, 1990). For the simultaneous estimation of the model parameters, generally two methods can be used, a modified simplex search algorithm after Nealder and Mead, and a Newton–Gaussian gradient algorithm. The Log Likelihood Function (LLF) is used as a merit function for the optimisation. The value of this function evaluates the kinetic model, in addition to parity plots (measured versus calculated rates or concentrations). Standard deviations of the estimated parameters indicate their significance.

3. Experimental results and discussion

3.1. Catalyst characterisation

Although a detailed investigation of the physico-chemical zeolite properties is not the focus of the present work, it is useful for the following kinetic studies as one basis for the development of the reaction network. Only with the knowledge of the catalyst characteristics, a mechanistic approach for the reaction kinetics can be explained and established.

The main characteristics of the zeolites before and after calcination and ion-exchange are shown in Table 1. The XRD patterns (not shown) are characteristic for the MFI structure and no additional crystalline phases can be detected. The total Si/Al ratio in the bulk of the parent sample (SN55, SM55) exhibits a value of 21.5 (XRF). It contains 0.05 wt.% Fe_2O_3 as impurities from the synthesis procedure. The ^{27}Al-NMR studies (not shown) indicate an octahedrally

Table 1
Results of the characterisation of the zeolites after different preparation stages

	Catalyst sample		
	Parent form/H-form	H-(Al)ZSM-5 (after 900 °C, 12 h)	Fe-(Al)ZSM-5 (after 900 °C, 12 h)
Si/Al_{bulk}	21.5	21.5	21.5
$Si/Al_{framework}$	22	80	n.d.
Brønsted acid sites (H^+, mmol/g)	0.669	0.088	n.d
Iron content (wt.%, Fe_2O_3)	0.05	0.05	1.9
Crystallinity (Q_{Al})[a]	0.91	0.84	0.84
Unit cell volume ($Å^3 \pm 3 Å^3$)[b]	5388	5371	5373
Micropore volume ($N\,cm^3$ /g)	0.143	0.128	0.153
Crystal size (μm)	2–3	2–3	2–3

[a] Method according to [36].
[b] Calculated from XRD pattern [20].

coordinated extraframework Al content <2%. Therefore, the Si/Al ratio in zeolite framework is approximately the same as in bulk.

After calcination at 900 °C for 12 h, a loss of crystallinity (Q_{Al}) and a contraction of the calculated unit cell volume occurred for both samples, which gives the first hint concerning the dealumination of the zeolite framework [35]. Brønsted acidity decreases, which is confirmed by the decrease of the amount of desorbed ammonia in the high temperature region (NH_3-TPD, $T > 250$ °C) [37]. In addition, the amount of tetrahedrally coordinated aluminium (^{27}Al-NMR, 55 ppm) decreases, which leads to an increase of framework Si/Al-ratio and the formation of extraframework aluminium. This is supported by the loss of micropore volume after the calcination procedure [35]. DRIFTS studies in [20] also confirm in a semi-quantitative way that the Brønsted acidic hydroxyl groups almost disappear. Moreover, the terminal silanol bands increase indicating the formation of defect sites as silanol nests in the zeolite framework after the calcination.

A more detailed study of the influence of the calcination procedure on the physico-chemical and catalytic properties of this zeolite in the benzene hydroxylation have previously been published [20]. It has been found that this treatment already leads to a dehydroxylation and dealumination of the same sample (H-(Al)ZSM-5) at calcination temperatures higher than 700 °C without any presence of steam. These results are confirmed by the basic research of Hong and Fripiat concerning high temperature calcination of ZSM-5 zeolites [35]. Thus, it has to be mentioned that it is generally not possible to differentiate if extraframework aluminium [9], dehydroxylated framework aluminium [8] or the low amount of iron [6] are the active sites in the calcined H-(Al)ZSM-5 responsible for the benzene hydroxylation. Nevertheless, it is a fact that activity and selectivity could be enhanced with increasing calcination temperature and time [7,8,31] reaching for the chosen zeolites an optimum after 12 h at 900 °C [20]. In our earlier studies, particularly, the loss of acidity (Brønsted sites) and zeolite polarity (dealumination), respectively, have been made responsible to favour activity and selectivity because of a decreasing interaction of the hydroxylated products (particularly phenol) with the zeolite. Thus, product inhibition and non-selective consecutive reactions starting from phenol could be diminished [20,31].

The ion-exchange with $Fe(NO_3)_3$ introduces additional iron in the zeolite (1.9 wt.% Fe_2O_3), which leads to a Fe/Al-ratio of 0.35. This value corresponds with the literature results using similar procedures [32–34]. A detailed characterisation of the generated iron species was not possible, so far. But according to the literature, a mixture of different iron species (nanoclusters, iron cations and other iron oxide particles) has been possibly formed [32–34]. Bulky iron oxide species (e.g. hematite) observed by Kögel et al. [44] after a solid state exchange are not visible in the present XRD pattern. From our XPS studies it has been concluded that iron species migrate into the zeolite channels during high temperature calcination. Using different ZSM-5 zeolites modified in the same way it has been shown that only iron species generated inside the zeolite can enhance phenol production without loosing long-term stability [31].

3.2. Preliminary process studies in fixed bed reactor (H-(Al)ZSM-5)

3.2.1. Influence of the feed composition on the selectivity–conversion behaviour

In preliminary investigations, the behaviour of the reaction system has been studied in the fixed bed reactor charged with H-(Al)ZSM-5 activated at 900 °C. In Figs. 2 and 3, the experimental results are shown as conversion–selectivity plots related to the converted benzene (Fig. 2) and to the converted N_2O (Fig. 3), respectively. Different symbols assign measurements of different reactant ratios in the feed. At the same feed composition, different data points are measured at different modified residence times (τ_{mod}) and at time-on-stream (TOS) of 15 min.

Starting from an equimolar feed composition of 1:1 ($x(N_2O) = 0.04$, $x(B) = 0.04$) an increasing excess of the molar fraction of benzene (N_2O:B < 1) leads to an increase of the phenol selectivity on the expense of the benzene conversion staying at one particular *S–X* trajectory (dotted lines in Figs. 2 and 3). The extrapolation of these trajectories towards zero benzene conversion ($X_B \rightarrow 0$) leads to a

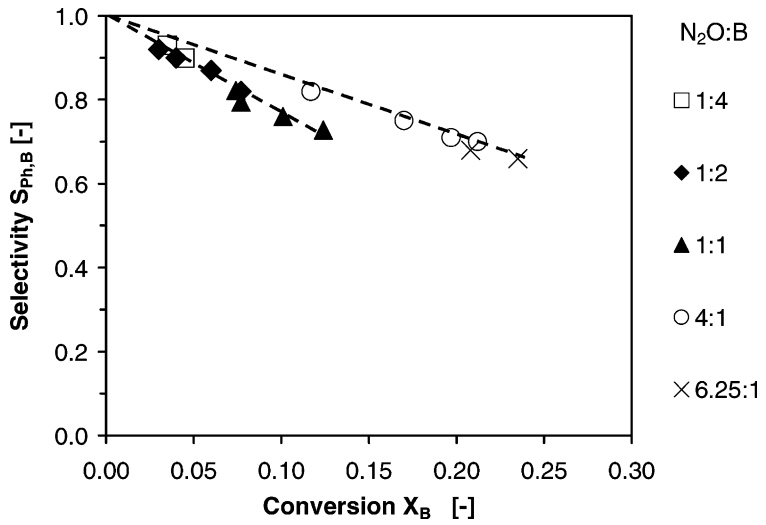

Fig. 2. Phenol selectivity related to converted benzene vs. benzene conversion. Influence of the N_2O:benzene feed concentration ratio using H-(Al)ZSM-5 in the fixed bed reactor; $\tau_{mod} = 78–156$ g min/mol, $T = 400$ °C, TOS = 15 min.

corresponding phenol selectivity of 100% ("catalyst selectivity" according to Riekert [45]). This allows the conclusion that neither any parallel side reactions starting from benzene nor a mass transport limitation of benzene in the zeolite crystal and pellets has to be considered [45]. The last result is also confirmed by the estimation of the Weisz module (Ψ). The diffusion coefficient for benzene in ZSM-5 zeolites has been measured, for example, by Masuda et al. [18] to 3.5×10^{-14} m^2/s at the present temperature of 400 °C. With a crystal size $d_C = 2$ μm, and an effective maximum rate for the molar consumption of benzene of 0.05 mmol/(g min), the maximum Weisz module, Ψ, is about 1. According to the Weisz–Prater criterion, the influence of internal mass transport on the observed reaction rate of almost zero reaction order (see Section 5) can be neglected ($\Psi < 6$) [46]. This is confirmed by the calculations of Louis et al. [29].

The decrease of conversion with increasing benzene feed concentration was first found by Burch and Howitt [47]. For the kinetic model, this behaviour leads to a fractional order related to the benzene concentration, which has already been applied in a power law model by our group [27,28] describing the experimental results on H-(Ga)ZSM-5. However, it has also been pointed out that a more satisfying description can only be reached using a model, which considers the sorption of the reactants and products [27]. Thus, an obvious displacement of phenol by benzene in the adsobate phase can be introduced into the kinetic model [48].

With an excess of N_2O (N_2O:B > 1), phenol selectivity slightly, but significantly, increases at comparable benzene

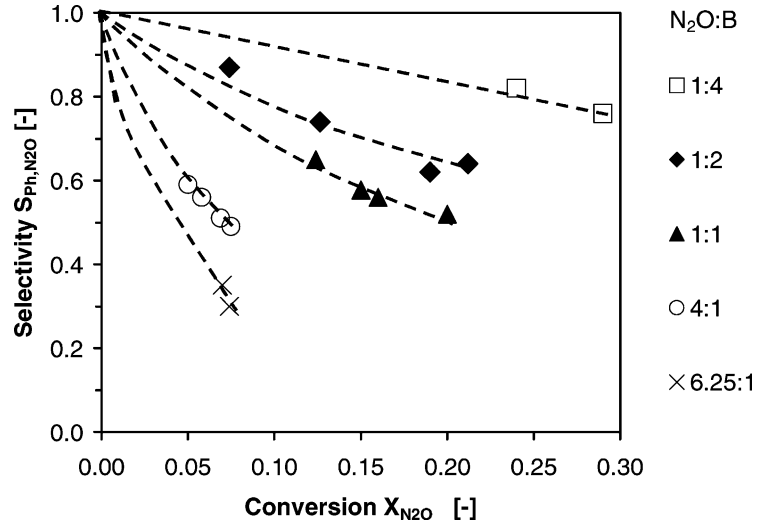

Fig. 3. Phenol selectivity related to converted N_2O vs. N_2O conversion: Influence of the N_2O: benzene feed concentration ratio using H-(Al)ZSM-5 in the fixed bed reactor; $\tau_{mod} = 78–156$ g min/mol, $T = 400$ °C, TOS = 15 min.

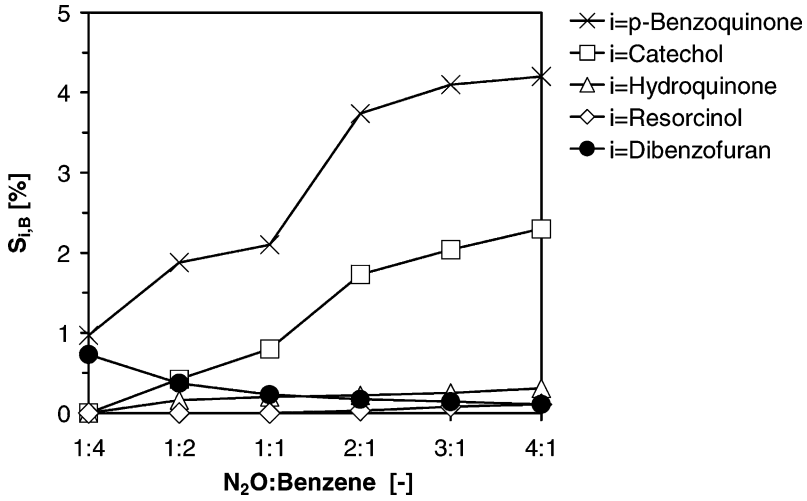

Fig. 4. Selectivities to by-products related to converted benzene vs. N_2O:benzene feed concentration ratio using H-(Al)ZSM-5 in the fixed bed reactor; $\tau_{mod} = 156$ g min/mol, $T = 400\,^{\circ}C$, TOS = 15 min.

conversions. These results indicate that phenol formation is stronger dependent on the N_2O concentration than any consecutive reaction of phenol.

The *X–S* behaviour related to the conversion of the oxidant N_2O (see Fig. 4) has almost never been mentioned in literature, so far, though it is of particular importance [21]. In the present case, it can be realised that with decreasing N_2O:benzene ratio, the phenol selectivity related to the converted N_2O increases compared at the same N_2O conversion. Thus, the rate for the reaction of benzene with the chemisorbed oxygen forming phenol must be higher than the oxygen consumption in consecutive reactions.

In these first process studies, in the fixed bed reactor the question arises, which by-products are formed and how their formation is influenced by the feed composition.

3.2.2. *By-products and element balances*

Fig. 4 shows that the by-products can only be detected in minor amounts at time-on-stream of 15 min. It should be mentioned that no CO_2 is formed, even at a high N_2O surplus. The by-products result, on the one hand, from a consecutive phenol hydroxylation forming diphenols and *p*-benzoquinone. Thereby, the formation of catechol and *p*-benzoquinone dominates, which results from the directing effect of the hydroxyl group of phenol. Hydroquinone is subsequently oxidised to *p*-benzoquinone, which exhibits the highest formation rate among all detectable by-products.

On the other hand, products of dimerisations, condensations and oxidative coupling can be detected. Phenoxyphenol, diphenylether (both in traces) and dibenzofuran could clearly be identified. Fig. 4 indicates that an excess of benzene slightly enhances the formation of dibenzofuran. Burch and Howitt have also detected these kind of products extracting coke species from the zeolites after hydroxylation experiments [49]. In this way, it has been demonstrated that bulky oxygenated products have still been adsorbed in the zeolite crystals.

However, it becomes clear that the element balance - carbon and oxygen - cannot be fulfilled taking into account the sum of by-products. Fig. 5 exemplarily shows an integral carbon balance at a modified residence time of 156 g min/mol after a time-on-stream of 100 min. This cannot represent the stationary measurements at TOS = 15 min, but it demonstrates what happens with increasing processing time. Although phenol is obviously the major product with a relative amount in all identified products of more than 95%, its selectivity related to the converted benzene does not exceed 90%. In regeneration with air after the hydroxylation experiment, surface bound carbon detected via CO_2 formation in the micro-gas chromatograph (see Section 2.2) can be quantified, but its amount is not high enough to close the carbon balance. An explanation could be the loss of adsorbed hydrocarbons during heating up to the regeneration temperature of 500 °C in nitrogen. This corresponds to the results of Burch and Howitt who found after benzene hydroxylation, soft and hard coke species in the zeolite, which can be removed in nitrogen and air atmosphere, respectively [49]. Conclusively, the carbon balance must be fulfilled by adsorbed phenol, which is accumulated inside the zeolite and/or is consumed by consecutive oligomerisation reactions only slightly depending on the N_2O-concentration (see Fig. 5).

The oxygen balance (not shown) is even worse fulfilled than the carbon balance. Increasing the N_2O:benzene ratio from 1:4 to 4:1 the amount of oxygen, which can be found in the products decreases from 80 to 50%. These values also consider water, which is formed by the oxidative dehydrogenation of hydrochinon, oxidative coupling and condensation reactions. Water formation has only been calculated because it cannot be quantified by gas chromatography analysis. The oxygen balance is much strongly dependent on the N_2O concentration than the carbon balance. This

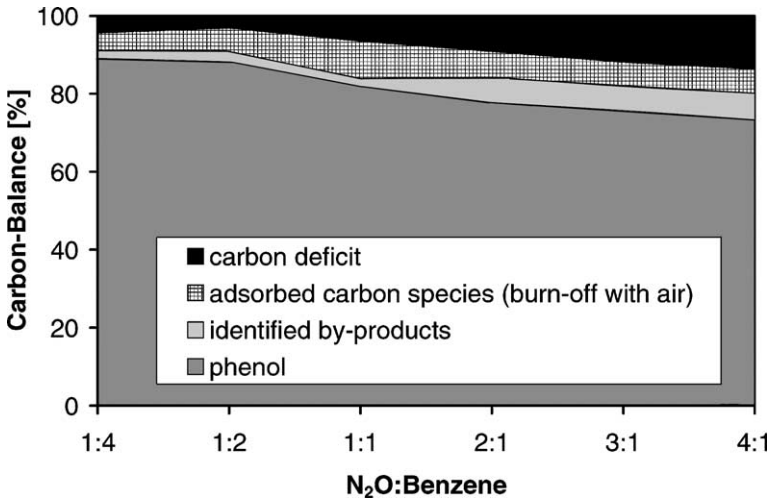

Fig. 5. Integral carbon balance and product distribution vs. N_2O: benzene feed concentration ratio using H-(Al)ZSM-5 in the fixed bed reactor; $\tau_{mod} = 156$ g min/mol, $T = 400\,^{\circ}C$, TOS ≤ 100 min.

indicates that a significant amount of oxygen must be stored in coke species formed inside the zeolite. Our experiments in [20] supported this assumption because a certain amount of CO_2 is formed when purging the catalyst bed in nitrogen at a temperature of 500 °C after the hydroxylation reaction. This result has also been confirmed by following the catalyst regeneration with DRIFT spectroscopy. Therefore, we concluded that coke, which stored the oxygen thermally decomposes because of the absence of an oxidising atmosphere. In Section 3.3, this effect will be discussed further, analysing the kinetic measurements in the CSTR.

3.3. Kinetic studies in the recycle reactor

The well-known advantage of an ideally CSTR in kinetic investigations is the possibility to measure directly, the molar rates of reactant consumption and product formation at definite process conditions. Moreover, an isothermal catalyst bed can be better ensured and so any formation of hot-spots can be avoided because of high gas velocities. The on-line measurement of the temperature gradient across the catalyst bed confirms that it never exceeds 2 K neither for H-(Al)ZSM-5 nor for Fe-(Al)ZSM-5 under any process conditions.

3.3.1. Dependencies of the molar rates using H-(Al)ZSM-5

Fig. 6 displays the molar rates (R_i) of N_2O and benzene consumption and phenol formation on H-(Al)ZSM-5 as a function of the corresponding reactant concentration (as molar fraction) inside the reactor at a time-on-stream of 15 min. Generally, the following important results can be found:

- All molar rates show a saturation dependency on the molar fraction of N_2O in the reactor and the plateau of constant rate is reached at $x(N_2O) \sim 0.12$ (Fig. 6A).

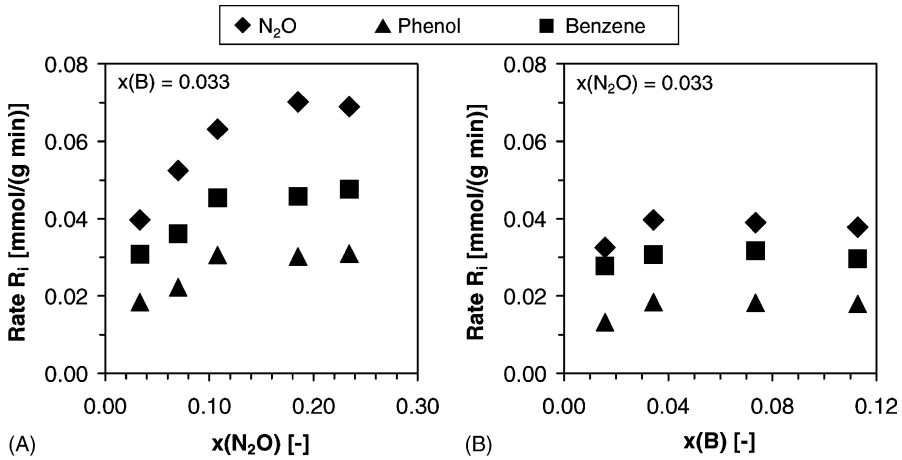

Fig. 6. Molar rates of benzene (R_B) and N_2O (R_{N_2O}) consumption and phenol formation (R_{Ph}) vs. molar fractions of the reactants in the recycle reactor using H-(Al)ZSM-5. (A) N_2O ($x(N_2O)$) and (B) benzene ($x(B)$); $\tau_{mod} = 137$ g min/mol, $T = 400\,^{\circ}C$, TOS = 15 min.

Therefore, it can be assumed that a sorption equilibrium is preceded before the reaction itself takes place, which can be described by the Langmuir theory.

- At molar fractions of benzene, $x(B) > 0.04$, all molar rates are almost independent on $x(B)$ (Fig. 6B). This leads to the assumption that saturation of the benzene adsorption is reached inside the micropore system of the zeolite. Therefore, an increase in the benzene concentration in the gas phase has no influence on benzene consumption. In Section 3.2.1, it has already been shown that the diffusion of benzene has no influence on its consumption rate and sorption equilibrium should be reached in the whole zeolite crystal.
- Less phenol is produced than stoichiometrically expected from benzene consumption ($R_B > R_{Ph}$). The formation rates of the by-products are very low (mainly, *p*-benzoquinone (not shown): $R_{BQ} < 0.002$ mmol/(g min)) and the carbon deficiency is nearly independent on molar fraction of N_2O and benzene. In Section 3.2.2, this consumption of phenol has already been identified as responsible for the loss of phenol selectivity related to benzene. It can result from a proceeding accumulation of phenol and/or oligomerisation reactions to coke or coke precursors. So, generally a consecutive reaction of phenol without the participation of N_2O has to be considered for the kinetic model.
- The N_2O consumption is higher than stoichiometrically necessary for the phenol production ($R_{N_2O} > R_{Ph}$). This difference increases with increasing molar fraction of N_2O (Fig. 6A). Since no formation of by-products (oxygenates or CO_2) could justify the lack of oxygen, phenol has to be accumulated in oligomerised aromatic hydrocarbons and coke species by their further oxygenations, respectively. These conclusions have also been drawn interpreting the experimental results in the fixed bed reactor (see Section 3.2.2).

3.3.2. Dependencies of the molar rates using Fe-(Al)ZSM-5

The catalytic behaviour of Fe-(Al)ZSM-5 corresponds to that of H-(Al)ZSM-5 concerning the following points up to a molar fraction $x(N_2O)$ of 0.18, after which CO_2 formation starts (see Fig. 7A):

- All molar rates of consumption and production show a saturation dependency concerning the molar fraction of N_2O in the reactor (see Fig. 7A).
- The consumption of N_2O and benzene is higher than stoichiometrically necessary for the phenol formation, which leads to the already described element deficits and their consequences. Thereby, carbon deficit is nearly independent of the molar fraction of N_2O, the oxygen deficit increases with increasing amount of N_2O in the reactor. The mainly detectable byproduct is *p*-benzoquinone before total oxidation occurs (not shown: $R_{BQ} < 0.03$ mmol/(g min)).

So, on the one hand, a N_2O-independent accumulation and oligomerisation of phenol and on the other hand, a N_2O-dependent accumulation and storage of oxygen within the coke species are again the most important side reactions on this catalyst.

However, some differences between the behaviour of Fe-(Al)ZSM-5 and H-(Al)ZSM-5 are also obvious:

1. All molar rates using Fe-(Al)ZSM-5 are significantly higher than on H-(Al)ZSM-5, but carbon and oxygen deficits are also higher. Additionally, the oxygen deficit is strongly dependent on the molar fraction of N_2O. This indicates that the non-selective consumption of oxygen by coke oxygenation is now enhanced.
2. At molar fractions higher than 0.18 for N_2O, the formation of carbon dioxide abruptly starts on Fe-(Al)ZSM-5 (see Fig. 7A). The increase of the corresponding rate to 0.04 mmol CO_2/(g min)) should lead to an increase of the

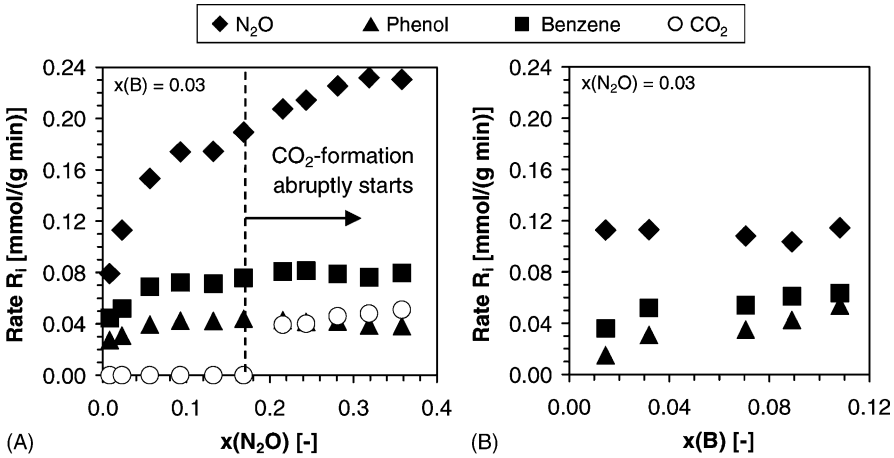

Fig. 7. Molar rates of benzene (R_B) and N_2O (R_{N_2O}) consumption and phenol formation (R_{Ph}) vs. molar fractions of the reactants in the recycle reactor using Fe-(Al)ZSM-5. (A) N_2O ($x(N_2O)$) and (B) benzene ($x(B)$); $\tau_{mod} = 137$ g min/mol, $T = 400\,^{\circ}C$, TOS = 15 min.

molar rate of N_2O consumption of 0.08 mmol/(g min) because of the stoichiometry. This is definitely not observable. Thus, the necessary amount of oxygen must result, in parts, from the coke species itself. After this sudden start, the increase of N_2O consumption is nearly twice of the CO_2 formation, which means that N_2O is now directly used for the total oxidation and no further oxygen storage occurs. Simultaneously, also the phenol formation rates slightly decrease, which leads to the assumption that part of the phenol is also directly oxidised to CO_2.

3. The molar rates of benzene consumption and phenol formation increase with increasing molar fraction of benzene while the N_2O consumption is almost constant (see Fig. 7B). The question arises now whether a sorption equilibrium as for H-(Al)ZSM-5 could also be used as an adequate model assumption. The idea of a competitive sorption of benzene and phenol [48] could explain this behaviour. If excess of benzene displaces phenol from its surface bound status, the coverage of benzene increases and enhances the phenol formation in this way. Simultaneously, the higher rate of selective oxygen consumption for phenol formation should result in an increasing phenol selectivity.

4. Derivation of the reaction network and the kinetic model

4.1. Reaction network

All results derived from the experimental studies using both catalysts can be concluded in an extended reaction network, which is shown in Fig. 8:

First benzene and N_2O adsorb in the zeolite, Z, which is represented by the corresponding sorption equilibria. N_2O is activated upon the formation of a monoatomic oxygen species at an active site Z_1 under the release of nitrogen. A suggestion for the different active sites will be given in the following section on the basis of the catalyst characterisation (see Table 1) and the knowledge collected from additional studies and literature.

Apart from the hydroxylation of adsorbed benzene by the chemisorbed oxygen species as the main reaction (MR), the consecutive reaction of phenol without the participation of chemisorbed oxygen (side reaction of phenol 1, SP1) and the non-selective oxygenation of adsorbed hydrocarbons by chemisorbed oxygen (side reaction of N_2O, SN) have to play an important role for the decrease of the corresponding selectivities:

- SP1 should be attributed to the accumulation of phenol inside the ZSM-5 crystal due to strong adsorption and slow diffusion of phenol, which subsequently leads to oligomerisation products ($C_xH_yO_z$). Transient studies in the TAP reactor [12] and in the fixed bed reactor separating oxidation and reduction steps [20] have supported these ideas. In these investigations, phenol has been detected strongly in the delayed in gas phase though the reactants, benzene and N_2O, are immediately and totally consumed. It has also been found that this effect is dependent on the reaction temperature enhancing the desorption and diffusion of phenol. However, after those experiments, a small amount of coke could be burned off only with air indicating the formation of hard coke species inside the zeolite, which has also been found by Burch and Howitt [49].
- SN results in an accumulation and storage of oxygen within those strongly adsorbed coke species ($C_xH_yO_{z+1}$) until a critical oxygen content is reached and total oxidation starts. At high molar fractions of N_2O, a direct oxidation of phenol to CO_2 by chemisorbed oxygen also occurs. The dotted arrows indicate that it has been not possible to introduce the total oxidation into the model.
- Additional side reactions of phenol and chemisorbed oxygen with minor importance are the consecutive hydroxylation of phenol by oxygen to diphenols and *p*-benzoquinone designated as SP2 (side reaction of phenol 2).

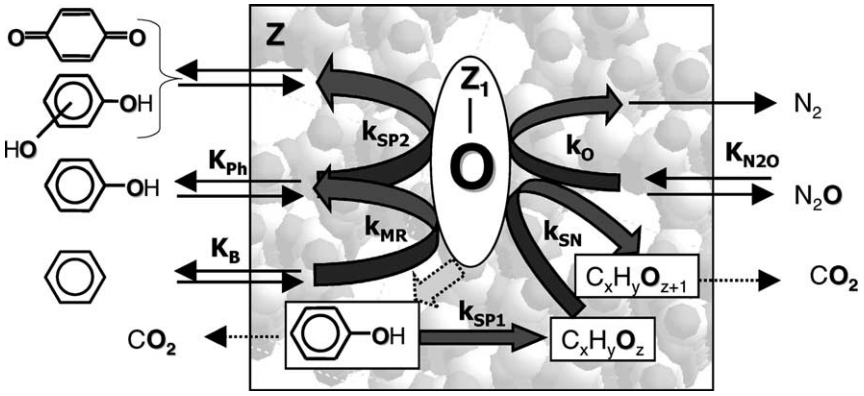

Fig. 8. Derived reaction network for the benzene hydroxylation including relevant mechanistic steps as basis for the kinetic model with corresponding model parameters.

4.2. Kinetic model: equations and assumptions

On the base of the experimental results in the CSTR and the reaction network in Fig. 9 the kinetic model can be developed in terms of model equations:

(A) *Sorption equilibria of N_2O and benzene in the micropore system of the zeolite Z*:

$$N_2O \rightleftharpoons Z\text{-}N_2O \tag{3}$$

$$B + Z \rightleftharpoons Z\text{-}B \tag{4}$$

Additionally, it is assumed that sorption equilibrium of phenol is also reached

$$Ph + Z \rightleftharpoons Z\text{-}Ph \tag{5}$$

If this is not true or the desorption is the rate determining step, a lack of fit must result. Although it is difficult to specify the site Z in more detail, acidic sites (predominately, Lewis sites, but also the remaining Brønsted sites (see Section 3.1)) must be responsible for the sorption, also for N_2O [50]. With the pretreatment procedure (high-temperature calcination), the sorption properties are adjusted in the right way by diminishing the Brønsted sites [20].

The sorption is described by the Langmuir theory resulting in the surface coverages

$$\theta_{Z,B} = \frac{K_B\, x(B)}{1 + K_B\, x(B) + K_{Ph}\, x(Ph) + K_{N_2O}\, x(N_2O)} \tag{6}$$

$$\theta_{Z,Ph} = \frac{K_{Ph}\, x(Ph)}{1 + K_B\, x(B) + K_{Ph}\, x(Ph) + K_{N_2O}\, x(N_2O)} \tag{7}$$

Since the sorption constant of N_2O is very small compared with those of the aromatics, sorption of N_2O should not influence the interaction of the aromatics. Therefore, "$K_{N_2O}\, x(N_2O)$" in Eqs. (6) and (7) can be neglected. This assumption is supported by Cerius[2] simulations resulting in $K_{N_2O} = 0.15\, K_B$ [27,28]. In this way, a competitive sorption of the aromatics, benzene and phenol, at the same site is introduced into the model. The sorption of any by-products (oxygenates) is neglected, because at TOS = 15 min, their formation is still very low.

Figs. 6B and 7B display that the saturation of benzene and phenol coverage is reached. Therefore, the "1" in Eqs. (6) and (7) can be neglected, which means that free sorption sites are no more available ($\theta_{Z,free} = 0$). This leads to the following expressions for the surface coverages for the aromatics

$$\theta_{Z,B} = \frac{1}{1 + (K_{Ph}\, x(Ph)/K_B\, x(B))} \tag{8}$$

$$\theta_{Z,Ph} = \frac{1}{1 + (K_B\, x(B)/K_{Ph}\, x(Ph))} \tag{9}$$

The last assumption will be checked after estimation of the kinetic parameters in Section 5.1.

(B) *Activation of adsorbed N_2O leading to the formation of chemisorbed oxygen species at the site Z_1*:

$$Z\text{-}N_2O + Z_1 \rightarrow Z + N_2 + Z_1\text{-}O \tag{10}$$

Although it has been assumed that the sorption of N_2O has no influence on the interaction of aromatics with zeolite, a sorption equilibrium for N_2O has to precede the formation of the chemisorbed oxygen species. This becomes clear from the characteristic dependency of the rates on increasing N_2O concentration in the CSTR (Figs. 6A and 7A). This idea leads to the following introduction of an independent surface coverage of N_2O, which can be interpreted as a sorption of N_2O in the zeolite saturated with aromatics

$$\Theta_{Z,N_2O} = \frac{K_{N_2O}\, x(N_2O)}{1 + K_{N_2O}\, x(N_2O)} \tag{11}$$

Without this assumption, fitting of the experimental data was not successful. Louis et al. [29] have come to similar conclusions in their kinetic studies introducing two distinct, independent sites for N_2O and the aromatics. However, a clear designation of those sites has not been given.

Adsorbed N_2O dissociates at an active site (Z_1) under the formation of the chemisorbed oxygen species and nitrogen (rate r_O)

$$r_O = k_O \Theta_{Z,N_2O}\, \alpha_{Z_1,free} \tag{12}$$

$$\alpha_{Z_1,O} + \alpha_{Z_1,free} = 1 \tag{13}$$

The site Z_1 probably represents a special iron species, which is present in traces in H-(Al)ZSM-5 and is increased by iron-exchange in Fe-(Al)ZSM-5 according to Panov et al. [4,6] and Dubkov et al. [14]. This would explain the higher consumption rates on iron exchanged ZSM-5. On the other hand, Lewis acidic defect sites in the framework, which are generated by the high temperature calcination can additionally stabilise the active oxygen species [8] (see Section 3.1). This could explain the high activity of H-(Al)ZSM-5, where iron is present only in traces. Therefore, a decision if iron in the zeolite is *essentially* necessary for phenol formation is again not possible. Even a "symbiotic" combination of both types of active sites cannot be excluded.

(C) *Consumption of the chemisorbed oxygen*:

(C1) *Main reaction (MR)*:

$$r_{MR} = k_{MR}\, \alpha_{Z_1,O}\, \theta_{Z,B} \tag{14}$$

(C2) *Side reaction (SN)*:

$$r_{SN} = \hat{k}_{SN}\,\alpha_{Z_1,O}\,\theta_{Z,C_xH_yO_z} \quad (15)$$

(D) *Consumption of phenol (accumulation, oligomerisation: SP1)*:

$$r_{SP1} = k_{SP1}\,\theta_{Z,Ph} \quad (16)$$

(E) *Consecutive hydroxylation (formation of p-benzoquinone: SP2)*:

$$r_{SP2} = k_{SP2}\,\alpha_{Z_1,O}\,\theta_{Z,Ph} \quad (17)$$

These equations contain as unknown and non-measurable quantities the coverages of oxygenate ($\theta_{Z,C_xH_yO_z}$) and chemisorbed oxygen ($\alpha_{Z_1,O}$). The pseudo-species oxygenate comprises different oxygen containing species (except for phenol and *p*-benzoquinone), which are bound to the surface. It can be assumed that at TOS = 15 min sufficient oxygenate species are present that r_{SN} is no more dependent on $\theta_{Z,C_xH_yO_z}$. This simplifies Eq. (15) to

$$r_{SN} = k_{SN}\,\alpha_{Z_1,O} \quad (18)$$

The coverage of chemisorbed oxygen ($\alpha_{Z_1,O}$) is eliminated by Bodenstein's steady-state approximation. Thus, the formation rate (Eq. (12)) and main consumption rates (Eqs. (14) and (18)) are set equal and together with the site balance (Eq. (13)) the unknown oxygen coverage can be calculated according to

$$\alpha_{Z_1,O} = \frac{k_O}{k_{MR}\theta_{Z,B} + k_{SN} + k_O\Theta_{Z,N_2O}}\Theta_{Z,N_2O} \quad (19)$$

Applying Eqs. (8) and (11) the coverage of N_2O and benzene can be calculated. The consecutive hydroxylation (Eq. (17)) is not considered due to its negligible contribution to the overall reaction. Defining a new pseudo-rate constant $\hat{k}_O$ Eq. (19) can be transformed to

$$\alpha_{Z_1,O} = \hat{k}_O\Theta_{Z,N_2O} \quad (20)$$

The constant $\hat{k}_O$ represents the ratio between the rate constants of formation and consumption of chemisorbed oxygen. Its value allows the identification if the former [6] or the latter step is rate determining.

It was not possible to introduce the CO_2 formation into the model because according to the discussion in Section 3.3.2, the oxygen accumulation is a non-stationary phenomenon, which precedes the start of the total oxidation. Additionally, the oxygen content of the coke initiates the total oxidation. Therefore, the present steady-state approach cannot be successful.

The molar rates of N_2O and benzene consumption and phenol formation

$$-R_B = k_{MR}\,\alpha_{Z_1,O}\,\theta_{Z,B} \quad (21)$$

$$-R_{N_2O} = k_{MR}\,\alpha_{Z_1,O}\,\theta_{Z,B} + k_{SN}\alpha_{Z_1,O} + 2k_{SP2}\theta_{Z,Ph}\,\alpha_{Z_1,O} \quad (22)$$

$$R_{Ph} = k_{MR}\,\alpha_{Z_1,O}\,\theta_{Z,B} - k_{SP1}\,\theta_{Z,Ph} - k_{SP2}\,\theta_{Z,Ph}\,\alpha_{Z_1,O} \quad (23)$$

are expressed in detail by considering each coverage (θ_i, $\alpha_{Z_1,O}$)

$$-R_B = k_{MR}\,\hat{k}_O\frac{K_{N_2O}\,x(N_2O)}{1 + K_{N_2O}\,x(N_2O)} \times \frac{1}{1 + (K_{Ph}\,x(Ph)/K_B\,x(B))} \quad (24)$$

$$\begin{aligned}-R_{N_2O} = {} & k_{MR}\,\hat{k}_O\frac{K_{N_2O}\,x(N_2O)}{1 + K_{N_2O}\,x(N_2O)} \times \frac{1}{1 + (K_{Ph}\,x(Ph)/K_B\,x(B))} \\ & + k_{SN}\,\hat{k}_O\frac{K_{N_2O}\,x(N_2O)}{1 + K_{N_2O}\,x(N_2O)} \\ & + 2k_{SP2}\,\hat{k}_O\frac{K_{N_2O}\,x(N_2O)}{1 + K_{N_2O}\,x(N_2O)} \times \frac{1}{1 + (K_B\,x(B)/K_{Ph}\,x(Ph))}\end{aligned} \quad (25)$$

$$\begin{aligned}R_{Ph} = {} & k_{MR}\,\hat{k}_O\frac{K_{N_2O}\,x(N_2O)}{1 + K_{N_2O}\,x(N_2O)} \times \frac{1}{1 + (K_{Ph}\,x(Ph)/K_B\,x(B)K_B\,x(B))} \\ & - k_{SP1}\frac{1}{1 + (K_B\,x(B)/K_{Ph}\,x(Ph))} \\ & - k_{SP2}\,\hat{k}_O\frac{K_{N_2O}\,x(N_2O)}{1 + K_{N_2O}\,x(N_2O)} \times \frac{1}{1 + (K_B\,x(B)/K_{Ph}\,x(Ph))}\end{aligned} \quad (26)$$

5. Application of the kinetic model

5.1. Parameter estimation and quality of fit

With the SIMUSOLV software, the parameters of the kinetic model are estimated by fitting the experimental data measured in the CSTR by non-linear regression. Thereby, Eqs. (24)–(26) are simultaneously solved. For Fe-(Al)ZSM-5 only rates up to $x(N_2O)$ of 0.18 are used, because CO_2 formation has not been included in the model. The quality of fit for both catalysts is shown in Fig. 9 in the form of parity plots. The estimated parameters are depicted in Table 2.

The comparison of measured and calculated rates (see Fig. 9) shows that the model with the corresponding parameters fits the measured points well within a deviation of less than ±15% for H-(Al)ZSM-5 (see Fig. 9A) and less than ±20% for Fe-(Al)ZSM-5 (see Fig. 9B). All parameters are significant as can be seen from their standard deviations (see Table 2) and are not correlated to each other. Only the parameter $\hat{k}_O$ is strongly correlated to the other rate constants.

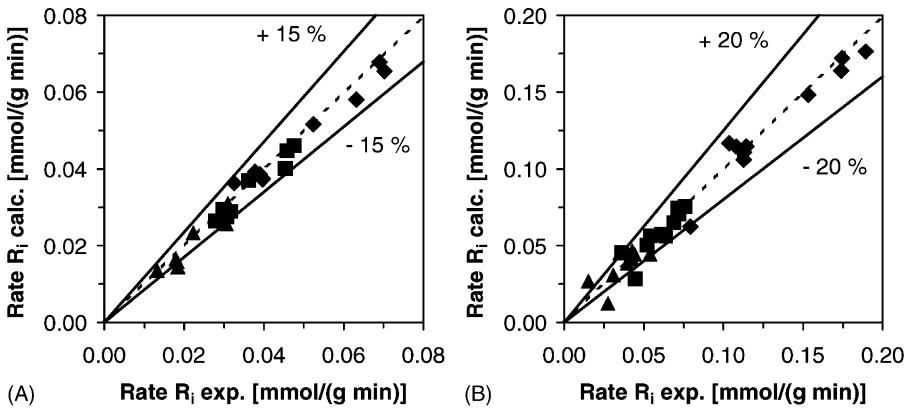

Fig. 9. Parity plots (calculated vs. measured rates) to the quality of the kinetic model. (A) H-(Al)ZSM-5 and (B) Fe-(Al)ZSM-5.

Thus, it has been fixed in several optimisation runs in a wide range (0.01–1000). It results that only if $\hat{k}_O$ has been set between 1 and 1000 the merit function (LLH) reaches maximum values, whereas all other parameters do not change significantly. Thus, it can be concluded that the formation of the chemisorbed oxygen from N_2O is fast enough for not being the rate determining step of the reaction network. Kinetic modelling of N_2O decomposition and N_2O reduction with CO on Fe-(Al)ZSM-5 zeolites by Kapteijn et al. [51] supports this result. In the present case, a more detailed description of parameter $\hat{k}_O$ is not possible because of the lack of experimental data.

The assumption that saturation has been reached for the aromatic hydrocarbons can be checked by using the complete equation for the surface coverage of benzene and phenol (Eqs. (6) and (7)). With that model the sorption constant for benzene (K_B) is always calculated in the range of 200–1000, which means that saturation is reached and almost no $\theta_{Z,free}$ are available.

Due to the assumed strong interaction of phenol with the zeolite, it has also been tried to set the phenol desorption as the rate determining step, which leads to new model equations. However, the desorption rate constant after fitting the experimental data is about one order of magnitude higher than the rate constant of the fastest surface reaction. Therefore, it can be excluded that the phenol desorption is rate determining.

Table 2
Estimated model parameters derived from the numerical fit of the recycle reactor data for different zeolite modifications

Parameter	H-(Al)ZSM-5		Fe-(Al)ZSM-5	
	Value	S.D.	Value	S.D.
$\hat{k}_O$	1–1000	–	1–1000	–
K_{N_2O}	28.5	2.8	33.1	2.7
K_{Ph}/K_B	1.3	0.5	7.1	0.8
k_{MR} (mmol/(g min))	6.5E−02	4.6E−03	0.211	9.3E−03
k_{SN} (mmol/(g min))	1.9E−02	1.8E−03	0.114	5.7E−03
k_{SP1} (mmol/(g min))	1.3E−02	8.4E−04	3.2 E−02	5.1E−03
k_{SP2} (mmol/(g min))	1.3E−02	1.6E−03	1.42 E−02	1.85E−04

5.2. Comparison between Fe-(Al)ZSM-5 and H-(Al)ZSM-5

Table 2 shows the influence of the catalyst modification on the kinetic parameters and on each single step of the reaction system.

The sorption constant for N_2O (K_{N_2O}) is almost equal on both catalysts. Thus, the exchange of iron has no influence on the sorption equilibrium of N_2O inside the zeolite. The rate constant (k_{MR}) for the phenol formation on Fe-(Al)ZSM-5 is more than three times higher than on H-(Al)ZSM-5. So, one would expect a higher phenol production and a higher selectivity related to converted benzene at Fe-(Al)ZSM-5. However, the higher ratio of the sorption constants on Fe-(Al)ZSM-5 ($K_{Ph}/K_B = 7.1$) than on H-(Al)ZSM-5 ($K_{Ph}/K_B = 1.3$) must also be considered. If the composition of the adsorbate is calculated for both catalysts at $x(B) \sim 0.016$ with Eqs. (8) and (9) H-(Al)ZSM-5 contains only 13 % phenol ($\theta_{Z,Ph} \sim 0.13$), in contrast to 50% on Fe-(Al)ZSM-5 ($\theta_{Z,Ph} \sim 0.5$). This means that an increasing iron content enhances the phenol interaction with the zeolite and promotes the phenol accumulation. The corresponding rate constant k_{SP1} confirms this conclusion because it is three times higher on Fe-(Al)ZSM-5 than on H-(Al)ZSM-5. So it becomes clear, that higher accumulation of phenol enhances formation of oligomers. Comparing both catalysts, the selectivity to phenol related to benzene at the same benzene conversion is always lower for Fe-(Al)ZSM-5 than for H-(Al)ZSM-5. This will be clearly demonstrated by the simulation of the selectivity–conversion behaviour (see Fig. 10) in the range of $\tau_{mod} = 0$–160 g min/mol, which will be discussed in detail in Section 5.3.

Sorption simulations with Cerius[2] in [19] support the results of the sorption constant ratio K_{Ph}/K_B obtained from the kinetic modelling. For H-ZSM-5 (Si/Al = 95) K_{Ph}/K_B has been calculated to be about 1.3 at the same reaction temperature of 673 K. Additionally, a slightly higher sorption enthalpy of phenol compared with benzene has resulted ($\Delta H_B = 58$ kJ/mol, $\Delta H_{Ph} = 63$ kJ/mol). Although the chosen zeolite in the present study in its parent form exhibits a

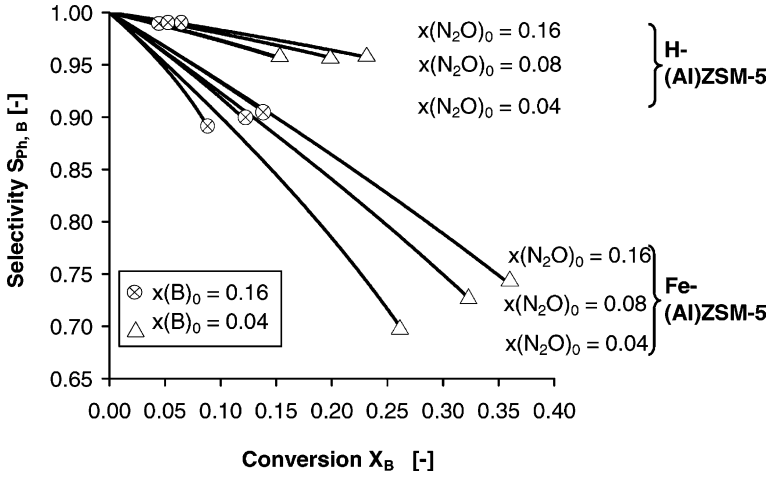

Fig. 10. Simulation of phenol selectivity related to converted benzene vs. benzene conversion for H-(Al)ZSM-5 and Fe-(Al)ZSM-5: influence of $x(N_2O)$ and $x(B)$; $\tau_{mod} = 0$–160 g min/mol, $T = 400\,^{\circ}C$, TOS = 15 min.

Si/Al ratio of 21–22, this value increases to about 80 after the calcination procedure (see Table 1). Therefore, the zeolite framework generated in the Cerius^2 simulation in [19] is quite similar to the calcined H-(Al)ZSM-5 of the present study. Additionally, it has been shown in [19] that the ratio K_{Ph}/K_B dramatically increases by a factor of 20, if there are any positive point charges (e.g. cations) in the zeolite (Na-ZSM-5, Si/Al = 95). The sorption enthalpy for phenol increases more distinctly than that for benzene ($\Delta H_B = 84$ kJ/mol, $\Delta H_{Ph} = 105$ kJ/mol). It can be expected that cationic ironoxospecies [32–34] have a similar effect on the phenol sorption. If these are the same species that generate the chemisorbed oxygen cannot be decided at the moment.

It has to be mentioned that phenol accumulation can also be caused by a inhibited transport of phenol out of the micropore system of the zeolite. Therefore, above all the crystal size, but also bulky extraframework aluminium and iron species (see Table 2) should have an influence on the macro-kinetic step of phenol diffusion. Experimental results by Ribera et al. [52] have shown a higher long-term stability with smaller crystals of H-(Fe)ZSM-5 ($d_C \sim 0.4\,\mu m$), which can be explained by an enhanced phenol diffusion. In particular, Vogel et al. have recently detected a strong crystal size effect in toluene hydroxylation to cresols with N_2O [53]. The selectivity to *p*-cresol has been increased reducing the crystal size by two orders of magnitude ($d_C = 2\,\mu m \rightarrow 0.05\,\mu m$). Thus, parameter k_{SP1} (accumulation of phenol) can also partly be related to phenol diffusion, though it is derived from a stationary model. When the kinetic model is applied to the experimental data of the fixed bed reactor (see Section 5.3) this question is further discussed.

The rate constant for the coke oxygenation (k_{SN}), which represents the non-selective N_2O consumption and oxygen accumulation, respectively, increases by a factor of 6 using Fe-(Al)ZSM-5 instead of H-(Al)ZSM-5. Thus, the phenol selectivity obtained with the latter sample at comparable N_2O conversions is generally higher (not shown). So it can be concluded that additional iron also enhances the non-selective N_2O consumption and oxygen accumulation in the coke, which finally leads to the CO_2 formation.

5.3. Simulation of the influence of feed composition

Fig. 10 demonstrates a simulation of the influence of the feed composition ($x(B)$, $x(N_2O)$) on phenol selectivities related to converted benzene in the range of $\tau_{mod} = 0$–160 g min/mol.

Phenol selectivity related to converted benzene increases, if the molar fraction of benzene is increased. This happens on the expense of benzene conversion moving back on almost the same *S*–*X* trajectory. It is obvious that this effect is more pronounced at Fe-(Al)ZSM-5 than on H-(Al)ZSM-5, which results from the stronger decrease of $\theta_{Z,Ph}$ when increasing feed concentration of benzene. The displacement of adsorbed phenol by an excess of benzene can be checked by calculating the change of the adsorbate composition. If $x(B)$ is increased from 0.02 to about 0.11, $\theta_{Z,Ph}$ decreases from 0.13 to 0.03 for H-(Al)ZSM-5, and from 0.5 to 0.33 on Fe-(Al)ZSM-5, respectively.

Increasing benzene concentration even leads to a slight decrease in phenol selectivity at comparable benzene conversions on Fe-(Al)ZSM-5. This supports that additional iron not only leads to higher phenol production, but also enhances the phenol accumulation and oligomerisation rate.

At a constant molar fraction of benzene, an increasing molar fraction of N_2O in the feed increases the selectivity to phenol related to converted benzene as it can also be seen in Fig. 2. So, the consumption of oxygen for the phenol formation is faster than the consumption in the coke oxygenation and oxygen accumulation, respectively. Nevertheless, high benzene feed concentrations are favourable for the phenol selectivity related to converted N_2O. It is already shown in Fig. 3 that the increase of S_{Ph,N_2O} is accompanied by

an increase in N_2O conversion. This is also pointed out by experimental studies of Panov et al. [21].

By comparing Figs. 2 and 10, the question arises for reason of the difference between measured selectivities in the fixed bed reactor and predicted ones derived from the model based on CSTR measurements. It has to be proven if the kinetic model can properly describe the PFR measurements.

5.4. Application of the kinetic model for simulating a fixed bed reactor

Generally, the kinetic model must be independent of the reactor model. This is verified by a comparison of the simulated and measured molar fractions at the reactor outlet in a range of $\tau_{mod} = 0$–160 g min/mol. For this purpose, exemplarily, the molar fractions of phenol are shown in Fig. 11A for three different N_2O:benzene ratios on H-(Al)ZSM-5. However, it becomes clear that the curvature of the measured points cannot be satisfactorily predicted by simulation. This means that along the reactor axis in the fixed bed reactor the phenol formation rate more strongly decreases than predicted. Obviously, the catalyst exhibits a higher level of activity in the fixed bed reactor than in the CSTR at a time-on-stream of 15 min. At the entrance of the PFR no phenol is present, whereas phenol exhibits a constant, high level in the whole CSTR. Since phenol, and not benzene, is the precursor for the coke formation, the catalyst in the CSTR is stronger deactivated after 15 min than in the PFR. A new parameter estimation using data measured in the fixed bed reactor leads to a much better fit of the experimental data, e.g. molar fractions of phenol (see Fig. 11B) and to a new set of significant parameters (see Table 3).

Now it becomes clear what has already been assumed. Almost all parameters including the ratio of the sorption constants, K_{Ph}/K_B, show higher values than from fitting the CSTR data. Thus, definitely the catalyst is at a higher activity level in the PFR than in the CSTR. The strongest influence is found for the rate constant, k_{SP1}, and the ratio of the sorption constants, K_{Ph}/K_B, which increase by a factor of 3.5 and 4.7, respectively. Therefore, phenol selectivities related to converted benzene are lower in the PFR (see Fig. 2) than predicted by the simulation derived from the CSTR data (see Fig. 10). Additionally, it becomes clear that those two parameters are related to each other in the way that a higher rate of accumulation increases the phenol coverage, which also decreases the total number of sorption sites by the enhanced formation of oligomers. Although the whole kinetic model is a steady-state approach, the parameters k_{SP1} and K_{Ph}/K_B seem to allow an estimation of the time-dependent status of the phenol accumulation, which has been mentioned in Section 5.2. Nevertheless, those parameters are still useful for the described estimation of phenol interaction with the catalyst dependent on its composition.

In conclusion, the transfer of the kinetic parameters from the CSTR to the PFR is only possible within certain limits, whereas the structure of the model derived from kinetic studies in the CSTR can be unrestrictedly transferred. For a detailed description of the fixed bed reactor behaviour, the model has to be extended by coke formation kinetics, which should be dependent on the local phenol concentration changing with time-on-stream. Moreover, the amount and composition of the oligomeric species must be specified

Table 3
Estimated model parameters derived from numerical fitting of the fixed bed reactor data for H-(Al)ZSM-5

Parameter	Value	S.D.
$\hat{k}_O$	1–1000	–
K_{N_2O}	28.7 (28.5)	2.4
K_{Ph}/K_B	4.5 (1.3)	0.7
k_{MR} (mmol/(g min))	0.11 (0.065)	6.4E−03
k_{SN} (mmol/(g min))	2.9E−02 (1.9E−02)	2.1E−03
k_{SP1} (mmol/(g min))	6.1E−02 (1.3E−02)	8.0E−03

Values in parentheses are parameters from the fit of the recycle reactor data.

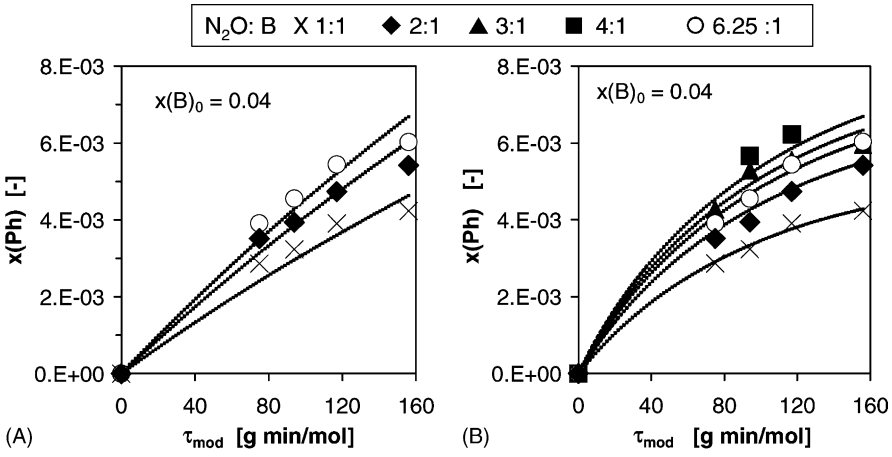

Fig. 11. Application of the kinetic model for prediction of data measured in a fixed bed reactor for H-(Al)ZSM-5. (A) Simulation with model parameters derived from CSTR (—) and (B) fit of the experimental values of the fixed bed reactor (—). Symbols are measured points in PFR.

in more detail to consider their surface coverage in the model. This work is in progress at the moment.

6. Conclusions

In the present study, a reaction network of the hydroxylation of benzene to phenol with nitrous oxide has been derived from kinetic measurements in a fixed bed reactor and a recycle reactor (Berty-type) varying the molar fractions of the reactants at a reaction temperature of 400 °C. Besides the formation of a chemisorbed, monoatomic oxygen species and its reaction with adsorbed benzene to phenol, a consecutive reaction of phenol without the participation of chemisorbed oxygen and a non-selective oxygenation of strongly adsorbed hydrocarbons by chemisorbed oxygen are important side reactions. These result, on the one hand, from the accumulation and oligomerisation of phenol inside the ZSM-5 crystal due to strong adsorption and slow diffusion of phenol, and on the other hand, from an accumulation of oxygen within the adsorbed aromatic species. The derived kinetic model contains two distinct terms for the competitive sorption of benzene/phenol and for the activation of N_2O. Although this has been supported by additional mechanistic investigations in earlier studies, no clear answer can be given to the question about the corresponding active sites. It is generally possible that Lewis acidic sites and iron species are responsible for generation of the chemisorbed oxygen species from N_2O, but iron should favour this reaction. The sorption of reactants and products, particularly the aromatics, refers to acidic sites. The model describes the measurements using a protonated and an iron-exchanged ZSM-5 zeolite with high accuracy. A comparison of the estimated kinetic parameters and the rates of each step, respectively, shows that the iron modification leads to higher phenol formation rate but also to a stronger phenol interaction with the catalyst resulting in higher accumulation and oligomerisation rate and a higher oxygen accumulation within the adsorbed hydrocarbon species. Therefore, both the phenol selectivities - related to benzene and to N_2O - of the iron modified zeolite never reach those of the unmodified sample. This can be demonstrated by simulations of the conversion–selectivity behaviour of both catalysts using the kinetic model. Moreover, the iron modification leads to carbon dioxide formation at high N_2O/benzene ratios in the reactor, which seems to start by a thermal decomposition of the oxygen saturated coke. This effect has experimentally been found, but it has not been possible to include it into the model, so far. The application of the kinetic model to the data measured in the fixed bed reactor shows its limitation concerning the deactivation starting from phenol. This non-steady-state reaction leads to the prediction of lower rates in the fixed reactor than measured because of the higher phenol concentration in the CSTR at the same time-on-stream. Therefore, the model has to be extended by coke formation kinetics, which is in progress at the moment.

Acknowledgements

We gratefully acknowledge the financial support of Phenolchemie GmbH. Additionally, we wish to thank Dr. Tanger, Dr. Weber and Dr. van den Tillart for many helpful discussions. We are also grateful to Dr. Tißler (Alsipenta GmbH) for the zeolite samples (SM55, SN55).

References

[1] J. Higgins, Chemical Engineering News, 31 May 1993, p. 23.
[2] European Chemical News, 22–28 May 2000, p. 28.
[3] A.K. Uriarte, M.A. Rodkin, M.J. Gross, A.S. Kharitonov, G.I. Panov, Stud. Surf. Sci. Catal. 110 (1997) 857.
[4] G.I. Panov, A.K. Uriarte, M.A. Rodkin, V.I. Sobolev, Catal. Today 41 (1998) 365.
[5] G.I. Panov, CATTECH 4 (1) (2000) 18.
[6] G.I. Panov, A.S. Kharitonov, V.I. Sobolev, Appl. Catal. A 98 (1993) 1.
[7] V.L. Zholobenko, I.N. Senchenya, L.M. Kustov, V.B. Kazanskii, Kinetika i Kataliz 32 (1) (1991) 132.
[8] L.M. Kustov, A.L. Tarasov, V.I. Bogdan, A.A. Tyrlov, J.W. Fulmer, Catal. Today 61 (2000) 123.
[9] J.L. Motz, H. Heinichen, W.F. Hölderich, J. Mol. Catal. A 136 (1998) 175.
[10] G.I. Panov, V.I. Sobolev, A.S. Kharitonov, J. Mol. Catal. 61 (1990) 85.
[11] V.I. Sobolev, G.I. Panov, A.S. Kharitonov, V.N. Romannikov, A.V. Volodin, K.G. Ione, J. Catal. 139 (1993) 435.
[12] E. Klemm, A. Reitzmann, G. Emig, S.A. Buchholz, H.W. Zanthoff, Erdöl Erdgas Kohle 12 (1999) 604.
[13] E. Klemm, A. Reitzmann, S.A. Buchholz, H.W. Zanthoff, Chem. Ing. Tech. 70 (1998) 1017.
[14] K.A. Dubkov, V.I. Sobolev, E.P. Talsi, M.A. Rodkin, N.H. Watkins, A.A. Shteinman, G.I. Panov, J. Mol. Catal. A 123 (1997) 155.
[15] P. Venuto, Micropor. Mesopor. Mater. 2 (1994) 297.
[16] R.F. Parton, J.M. Jacobs, D.R. Huybrechts, P.A. Jacobs, Stud. Surf. Sci. Catal. 46 (1989) 162.
[17] L. Forni, C.F. Viscardi, C. Oliva, J. Catal. 97 (1986) 469.
[18] T. Masuda, Y. Fujikata, T. Nishida, K. Hashimoto, Micropor. Mesopor. Mater. 23 (1998) 157.
[19] E. Klemm, J. Wang, G. Emig, Micropor. Mesopor. Mater. 26 (1998) 11.
[20] A. Reitzmann, G. König, F.M. Petrat, E. Klemm, G. Emig, DGMK Tagungsbericht 9903 (1999) 255.
[21] G.I. Panov, A.S. Kharitonov, G.A. Sheveleva, Patent WO 9527691 (1994), Patent US 5,672,777 (1997).
[22] M. Gubelmann, P.-J. Tirel, Patent EP 341165 (1992).
[23] L.M. Kustov, V.I. Bodgan, V.B. Kazansky, Patent EP 0 889 018 A1 (1999).
[24] J.L. Motz, W. Hölderich, H. Heinichen, Patent DE 196 34 406 A1 (1998).
[25] A. Reitzmann, G. Emig, E. Klemm, S. Kowalak, K. Nowinska, DE 19829515 A1 (2000).
[26] A.K. Uriarte, Stud. Surf. Sci. Catal. 130 (2000) 743.
[27] M. Häfele, A. Reitzmann, E. Klemm, G. Emig, Stud. Surf Sci. Catal. 110 (1997) 847.
[28] A. Reitzmann, H. Friedrich, E. Klemm, M. Häfele, G. Emig, in: M. Rozwadowski (Ed.), Proceedings of the 3rd Polish–German Zeolite Colloquium, Nicholas Copernicus University Press, Torun, 1998, p. 239.
[29] B. Louis, L. Kiwi-Minsker, P. Reuse, A. Renken, Ind. Eng. Chem. Res. 40 (6) (2001) 1454.
[30] A. Tissler, H. Schmidt, G. Winkhaus, K. Unger, EP 0406474 (1999).

[31] S. Kowalak, K. Nowinska, M. Swiecicka, M. Sopa, A. Jankowska, G. Emig, E. Klemm, A. Reitzmann, in: M.M.J. Treacy, et al. (Ed.), Proceedings of the 12th International Zeolite Conference, Materials Research Society, Warrendale, 1999, p. 1240.
[32] R. Joyner, M. Stockenhuber, J. Phys. Chem. 103 (1999) 5963.
[33] J. Cejka, B. Wichterlova, J. Krtil, M. Krivanek, R. Fricke, Stud. Surf. Sci. Catal. 69 (1991) 347.
[34] G. Centi, F. Vazzana, Catal. Today 53 (1999) 683.
[35] Y. Hong, J. Fripiat, Micropor. Mesopor. Mater. 4 (1995) 323.
[36] K.H. Bergk, W. Schwieger, in: Proceedings of the International Conference on Zeolites, Portoroz, 1984, p. 120.
[37] N.Y. Topsøe, K. Pedersen, E.G. Derouane, J. Catal. 70 (1981) 41.
[38] E. Klemm, M. Seitz, H. Scheidat, G. Emig, J. Catal. 173 (1998) 177.
[39] M. Baerns, H. Hofmann, A. Renken, Chemische Reaktionstechnik Vol. 2, Georg Thieme, Stuttgart, 1992.
[40] D.E. Mears, Ind. Eng. Chem. Process Des. Dev. 10 (4) (1971) 541.
[41] J.A. Moulijn, A. Tarfaoui, F. Kapteijn, Catal. Today 11 (1991) 1.
[42] H.F. Rase, Fixed-Bed Reactor Design and Diagnostics, Butterworths, Boston, 1990.
[43] G. Luft, H.A. Herbertz, Chem. Ing. Technol. 41 (11) (1969) S667.
[44] M. Kögel, R. Mönnig, W. Schwieger, A. Tissler, T. Turek, J. Catal. 182 (1999) 470.
[45] L. Riekert, Appl. Catal. 15 (1985) 89.
[46] P.B. Weisz, Z. Physik. Chem. 11 (1957) 1.
[47] R. Burch, C. Howitt, Appl. Catal. A 103 (1993) 135.
[48] M. Häfele, A. Reitzmann, D. Roppelt, G. Emig, Appl. Catal A 150 (1997) 153.
[49] R. Burch, C. Howitt, Appl. Catal. A 106 (1993) 167.
[50] V.L. Zholobenko, L.M. Kustov, V.B. Kazansky, in: R. von Ballmoos, J.B. Higgins, M.M.J. Treacy (Eds.) Proceedings of the 9th International Zeolite Conference, Butterworth, Montreal, 1993, p. 299.
[51] F. Kapteijn, G. Marban, J. Rodriguez-Mirasol, J.A. Moulijn, J. Catal. 167 (1997) 256.
[52] A. Ribera, I.W.C. Arends, S. de Vries, J. Perez-Ramirez, R.A. Sheldon, J. Catal. 195 (2000) 287.
[53] B. Vogel, C. Schneider, E. Klemm, Catal. Lett. 79 (1–4) (2002) 107.